Acta Pharmaceutica Sinica B 2026;16(1):337−351

Chinese Pharmaceutical Association
Institute of Materia Medica, Chinese Academy of Medical Sciences

Acta Pharmaceutica Sinica B

www.elsevier.com/locate/apsb
www.sciencedirect.com

ORIGINAL ARTICLE

Gambogenic acid ameliorates inflammation by inhibiting HK1-mediated Warburg effect and NLRP3 inflammasome activation in sepsis

Huanhuan Pang[a,b,*,†], Honglin Chen[c,†], Peng Chen[d,†], Xu Wei[e,†], Hongda Liu[b], Xueling He[a], Yang Yang[a], Junzhe Zhang[a], Dianfei Li[a], Linlin Lou[a], Wen Xie[c], Chong Qiu[a], Fei Xia[a], Qiuyan Guo[a], Shengnan Shen[a], Qiaoli Shi[a], Weiguang Li[a], Guang Han[c], Xijun Wang[b,*], Jigang Wang[a,b,f,*], Chengchao Xu[a,*]

[a]*State Key Laboratory for Quality Ensurance and Sustainable Use of Dao-di Herbs, Artemisinin Research Center, and Institute of Chinese Materia Medica, China Academy of Chinese Medical Sciences, Beijing 100700, China*
[b]*State Key Laboratory of Integration and Innovation of Classic Formula and Modern Chinese Medicine, Metabolomics Laboratory, Department of Pharmaceutical Analysis, Heilongjiang University of Chinese Medicine, Harbin 150040, China*
[c]*State Key Laboratory of Antiviral Drugs, School of Pharmacy, Henan University, Kaifeng 475004, China*
[d]*Experimental Research Center, China Academy of Traditional Chinese Medicine, Beijing 100700, China*
[e]*Wangjing Hospital, China Academy of Chinese Medical Sciences, Beijing 100700, China*
[f]*Department of Pulmonary and Critical Care Medicine, Shenzhen Institute of Respiratory Diseases, Guangdong Provincial Clinical Research Center for Geriatrics, Shenzhen Clinical Research Center for Geriatrics, Shenzhen People's Hospital, the First Affiliated Hospital, Southern University of Science and Technology, Shenzhen 518020, China*

Received 17 October 2024; received in revised form 21 February 2025; accepted 18 June 2025

KEY WORDS

Inflammation;
Activity-based protein profiling (ABPP);

Abstract Sepsis is a life-threatening disease caused by the dysregulated host immune response to infection, which eventually leads to multi-organ failure. Current therapeutic strategies rely heavily on antibiotics. However, conventional antimicrobial therapy often leads to antibiotic abuse and resistance. Therefore, it is of utmost importance to develop new agents for treating sepsis. Here, we demonstrated

*Corresponding authors.
E-mail addresses: jgwang@icmm.ac.cn (Jigang Wang), xijunw@sina.com (Xijun Wang), ccxu@icmm.ac.cn (Chengchao Xu), hhpang@icmm.ac.cn (Huanhuan Pang).
†These authors made equal contributions to this work.
Peer review under the responsibility of Chinese Pharmaceutical Association and Institute of Materia Medica, Chinese Academy of Medical Sciences.

https://doi.org/10.1016/j.apsb.2025.10.020

Target identification;
Chemical proteomics;
Gambogenic acid (GNA);
Hexokinase 1 (HK1);
Warburg effect;
Sepsis

that gambogenic acid (GNA) not only restricted the release of inflammatory cytokines in lipopolysaccharide (LPS)-stimulated macrophages but also attenuated the inflammatory response and organ damage in septic mice. By using the activity-based protein profiling (ABPP) strategy, we identified 30 potential target proteins of GNA. Among these potential targets, we found that GNA directly bound to the Cys684 residue of hexokinase 1 (HK1) and affected its enzyme activity and cellular localization. These findings were confirmed by the cellular thermal shift assay (CETSA), bio-layer interferometry (BLI), and single-site mutation experiments. Functionally, siHK1 alleviated the Warburg effect, suppressed the activation of NLRP3 inflammasome, and eventually suppressed the release of inflammatory cytokines. Taken together, our findings demonstrated that GNA could attenuate inflammation by alleviating HK1-mediated Warburg effect and NLRP3 inflammasome activation in sepsis and could serve as a novel therapeutic agent for sepsis and inflammatory disorders.

1. Introduction

Sepsis is a life-threatening disease with multi-organ dysfunction and high morbidity and mortality rates worldwide. Sepsis is commonly induced by deleterious infection and dysregulated immune function in the host[1-4]. Studies have shown that sepsis is the leading cause of global death, with a cumulative annual burden of up to 50 million patients and a mortality rate of more than 40%, wherein sub-Saharan Africa, Oceania, South Asia, East Asia, and South-East Asia bear the heaviest burden[5-7]. Although antibiotics, fluid resuscitation, and organ support strategies have been used for the treatment of sepsis in the clinic, limited therapeutic efficacy was achieved[8-10]. To make matters worse, clinical trials of several candidate drugs for the treatment of sepsis have failed to yield promising outcomes[11-13]. Therefore, it is important to further elucidate its precise mechanisms and develop new active small molecules to improve the treatment outcome of sepsis.

Patients with sepsis always harbor aberrant glucose metabolism compared to healthy individuals, which is manifested by the inability of cells to oxidize glucose through the tricarboxylic acid cycle and a preference towards aerobic glycolysis, increasing the level of lactic acid, a metabolic shift known as the "Warburg effect"[14,15]. Hexokinase (HK) is the rate-limiting enzyme of the glycolytic pathway, catalyzing the phosphorylation of glucose to produce glucose 6-phosphate, which is the starting point of the glycolytic pathway[16,17]. HK1 is located mainly on the outer mitochondrial membrane under normal physiological conditions[16,18]. It has been shown that the release of HK from the outer mitochondrial membrane promotes the activation of NLR family pyrin domain containing 3 (NLRP3) inflammasome in inflammatory diseases[19,20]. NLRP3 inflammasome is an important sensor in the innate immune system responsible for detecting exogenous pathogenic invasion and endogenous cellular damage[21]. NLRP3 inflammasome consists of NLRP3, cysteinyl aspartate-specific proteinase 1 (Caspase-1), and apoptosis-associated speck-like protein containing a CARD (ASC), where NLRP3 is responsible for trapping danger signals and recruiting downstream molecules. Caspase-1 is able to elicit the maturation of a variety of pro-inflammatory cytokines, such as interleukin-1β (IL-1β), and induce cellular pyroptosis, and ASC mediates the interaction between NLRP3 and Caspase-1[22,23]. Thus, targeting HK may be an attractive therapeutic strategy for the treatment of sepsis.

Natural products provide a treasure trove for the discovery of new drugs[24,25]. Gambogenic acid (GNA), a bioactive natural compound from the resin of *Garcinia hanburyi* Hook.f., has extensive pharmacological activities, such as anti-tumor and anti-fibrosis effects[26-31]. In addition, a previous study showed that GNA inhibited LPS-stimulated inflammation in macrophages[32]. However, the efficacy of GNA in protecting mice from sepsis-induced inflammation and multi-organ damage, as well as its anti-inflammatory targets and mechanisms, remains unclear. In the present study, we investigated the anti-inflammatory effects of GNA *in vitro* and *in vivo*, and explored the potential targets and mechanisms underlying its anti-inflammatory effects, providing novel insights and strategies for the treatment of sepsis.

2. Materials and methods

2.1. Mice experiment

Eight-week-old male BALB/c mice were bought from Viewsolid Biotech Co., Ltd. (Beijing, China). For all experiments, mice lived in a Specific Pathogen-Free (SPF) facility with 65%−70% humidity, 20−25 °C, and a 12-h light/dark cycle. Animal experiments were conducted following the guidelines and approval of the Institutional Animal Care and Use Committee and Animal Ethics Committee of the Institute of Chinese Materia Medica (approval number 2024B115).

To examine the effects of GNA on septic mice induced by CLP, 25 mice randomly were divided into 5 groups ($n = 5$ per group): Sham group, CLP group, GNA low-dose group (0.5 mg/kg/day), GNA medium-dose group (1 mg/kg/day), and GNA high-dose group (2 mg/kg/day). Prior to the CLP surgery, mice in GNA groups were intraperitoneally treated with different doses of GNA (CHB-X-130, ChromaBio, China; prepared in 0.5% CMC) once a day for successive 3 days, while the Sham and CLP groups received an equal amount of vehicle intraperitoneally. On the 4th day, except for the mice in the Sham group, the others underwent CLP surgery to induce the sepsis model. Briefly, mice were intraperitoneally injected with tribromoethanol solution (M2920, AibeiBio, China) at a dose of 10 μL per gram body weight, followed by disinfection of the abdominal skin under deep anesthesia, exposure and ligation of the cecum, and perforation of the ligated portion using an 18-gauge needle. Correspondingly, mice in the Sham group underwent a similar operation but did not experience ligation and puncture. Postoperatively, mice were immediately subcutaneously injected with 1 mL of saline for

recovery. Four hours post CLP surgery, mice in the GNA group were given 2 mg/kg GNA solution by intraperitoneal injection, while the other mice received solvent injections. After another 12 h, all mice were euthanized and sacrificed for blood and tissues (lungs, liver, spleen, intestines, kidneys) collection.

To observe the effects of GNA on the survival of septic mice induced by CLP, 30 mice were randomly divided into 3 groups ($n = 10$ per group): Sham group, CLP group, and GNA group. Prior to the CLP surgery, mice in the GNA group were given 2 mg/kg/day of GNA (prepared in 0.5% CMC) by intraperitoneal injection for 3 days, while mice in the Sham and CLP groups received vehicle intraperitoneally. Post the CLP surgery described above, the mortality rate of the mice within 48 h post-CLP was recorded, followed by euthanasia of the animals.

2.2. Serum biochemical analysis

The levels of TNF-α (ml002095, Mlbio, Shanghai, China), IL-1β (ml098416, Mlbio, Shanghai, China), IL-6 (ml063159, Mlbio, Shanghai, China), and lactic acid (ml205267, Mlbio, Shanghai, China) in mouse serum were detected using assay kits, following the corresponding manufacturer's instructions.

2.3. Pathological examination

Mouse tissues were fixed with 4% paraformaldehyde in PBS, dehydrated, embedded in paraffin, and sectioned at 4 μm thickness. The slices were treated sequentially with xylene and graded ethanol before staining with hematoxylin−eosin. Tissue histology images were viewed and photographed under a microscope.

2.4. Cell experiment

RAW264.7 cells were obtained from the Chinese National Cell Bank (Beijing, China). Cells were routinely cultured in Dulbecco's modified Eagle's medium supplemented with 10% fetal bovine serum (FBS) in an incubator at 37 °C with 5% CO_2 atmosphere. For the cell viability experiment, RAW264.7 cells were incubated in 96-well plates for 12 h, then GNA was added and incubated for another 24 h. Cell viability was assayed using the CCK-8 kit (C0038, Beyotime, Shanghai, China) as indicated in the instructions. For cells used for morphological observation, cells were inoculated into 6-well plates, and after the cells were attached to the wall, drugs and/or LPS (MB5198, Meilunbio, Dalian, China) were added and co-incubated with cells, and the cell morphology was observed under a light microscope.

2.5. Cytokines and metabolites measurement

RAW264.7 cells and cultured medium were collected. Intracellular L-lactic acid (BC2235, Solarbio, Beijing, China) levels and medium TNF-α (ml002095, Mlbio, Shanghai, China), IL-6 (ml063159, Mlbio, Shanghai, China), IL-1β (ml098416, Mlbio, Shanghai, China), and NO (BN27106, Biorigin, Beijing, China) levels were analyzed using the ELISA kits as prompted by the instructions.

2.6. Western blotting

RAW264.7 cells were collected and lysed. Protein concentrations were measured by a BCA assay kit (CW0014S, CWbio, Taizhou, China). Equal amounts of protein were separated by SDS-PAGE from different samples and transferred onto a PVDF membrane (IPVH00010, Millipore, MA, USA). After being blocked with 5% skimmed milk, the membranes were incubated with primary antibodies, including HK1 (A0533, ABclonal, Wuhan, China), NLRP3 (30109-1-AP, Proteintech, China), pro-Caspase-1 (AB179515, Abcam, UK), IL-1β (AB234437, Abcam, UK), ASC (A16672, ABclonal, China), MTCO2 (55070-1-AP, Proteintech, Wuhan, China), Tubulin (M1501-1, HuaBio, Hangzhou, China), and β-actin (AC026, ABclonal, Wuhan, China) overnight at 4 °C. After washing, the membranes were incubated with the corresponding secondary antibody. Blots were visualized using the enhanced chemiluminescence kit (MA0186-2, Meilunbio, Dalian, China) and semi-quantified using ImageJ software.

For Pull-down Western blot analysis, proteins were incubated with DBIA, precipitated with cold methanol, and then resuspended in PBS containing 0.2% SDS, followed by enrichment with streptavidin beads. The enriched proteins were denatured and dissociated from the beads at 95 °C and then subjected to immunoblotting as described above.

2.7. Quantitative real-time PCR

The total RNA was extracted from RAW264.7 cells using an RNA isolation kit (ET111-01, TransGen Biotech, China) and reversely transcribed into cDNA using a DNA synthesis kit (AT311-02, TransGen Biotech, China). Quantitative real-time PCR (RT-qPCR) was conducted using synthetic primers and SYBR Green on the QuantStudio 5 real-time PCR instrument (Applied Biosystems, Thermo, USA) coupled with StepOne software v2.3 following standard protocols. Primers for all genes in this study are listed in Supporting Information Table S1.

2.8. Protein competitive labeling experiments

For the live cell competitive labeling experiments, RAW264.7 cells were initially incubated with or without GNA for 2 h post LPS treatment for 12 h, and then treated with IAA-yne probe for 1 h. Cells were collected and lysed for protein extraction. Proteins were extracted by precipitation with pre-cooled acetone. After centrifugation, protein pellets were dissolved in loading buffer, denatured at 95 °C for 10 min, and separated by SDS-PAGE. Fluorescent gel images were acquired by Sapphire Biomolecular Imager (Azure Biosystems). Coomassie brilliant blue (CBB) staining was used as a loading control.

For the *in vitro* competitive labeling experiment, total proteins were extracted from RAW264.7 cells after LPS stimulation. Proteins were then co-incubated with or without competitors for 3 h, followed by incubation with the IAA-yne probe for click reaction, and finally subjected to gel electrophoresis.

2.9. ABPP-based target identification

RAW264.7 cells were treated with LPS and collected to extract total protein. The protein concentrations of each sample were measured by the BCA assay kit and adjusted to 2 mg/mL per sample. Then the protein extractions were incubated with or without GNA (500 μmol/L) for 3 h, followed by 1 h treatment with DBIA. Sequentially, proteins were reduced by DTT, alkylated with IAA, then precipitated with methanol/chloroform. The precipitates were dissolved in 400 μL of EPPS buffer (BN24148, Biorigin, Beijing, China), digested with trypsin at 37 °C overnight, labeled with TMT reagents, and incubated with streptavidin beads

at room temperature for 4 h. The streptavidin beads were washed with 0.1% formic acid in water (twice) and 0.1% formic acid in 50% acetonitrile/water (twice). The eluents were collected and concentrated to dryness by a speed vacuum concentrator at 45 °C. Peptide samples were resuspended in 0.1% formic acid in water and detected by an Orbitrap Fusion Lumos (Thermo Fisher Scientific) mass spectrometer coupled to an Easy-nLC1000 liquid chromatography system (Thermo Fisher Scientific) as previously described[73-77]. Two-tailed unpaired Student's *t*-tests followed by Benjamini−Hochberg FDR correction were performed to compare the levels of proteins between DBIA and DBIA + GNA groups. Proteins with $|\text{fold change}| > 2$ and adjusted P value (P_{adj}) < 0.01 were considered as differential proteins.

2.10. Cellular thermal shift assay

Total protein was extracted from LPS-treated RAW264.7 cells, and proteins were quantified and divided equally into two portions (1.5 mg/mL, 1 mL), incubated with GNA (80 μmol/L) or DMSO for 2 h at room temperature. Each protein sample was added to one of the 8 PCR tubes, heated at 8 different temperatures (42, 47, 52, 57, 62, 67, 72, and 77 °C) for 3 min, and then incubated in a thermal cycler at 4 °C for 3 min (Applied Biosystems, Inc.). The samples were centrifuged at 22,000×*g* for 20 min, then each supernatant was mixed with protein loading buffer and denatured at 95 °C for 10 min, followed by immunoblotting.

2.11. Intracellular imaging and immunofluorescence

RAW264.7 cells were cultured in a polylysine-precoated 4-chamber glass-bottom dish (D35C4-20-1-N, Cellvis, USA), pre-stimulated with LPS for 6 h, and then incubated with or without GNA. Cells were sequentially treated with 4% paraformaldehyde for 15 min and 0.2% Triton X-100 in PBS for 15 min, followed by incubation with 3% BSA in PBS for 60 min. Cells were incubated with primary antibody (1:300), followed by washing with PBS buffer, and then treated with a secondary fluorescent antibody (1:500). Imaging of immunostained cells was performed using a confocal laser scanning microscope (Leica TCS SP8 SR).

For the co-localization of probes and proteins within cells, follow the above steps until completing the GNA incubation. Subsequently, cells were incubated with IAA-yne for 1 h, fixed and permeabilized as described above, and click chemistry was performed for 1 h at room temperature, followed by antibody incubation and nuclear staining to treat the cells, and finally, cell imaging.

2.12. Molecular docking

The structure of GNA was obtained from PubChem (CID: 10794070), and the protein 3D structure of HK1 was downloaded from Alphafold (P17710). The docking between GNA and HK1 was performed by DeepMice (http://www.deepmice.com/). Docking results were analyzed and presented using Pymol (https://www.pymol.org/).

2.13. Enzyme activity

HK activity was measured by the HK activity assay kit according to the instructions. RAW264.7 cells were incubated with different concentrations of GNA or 15 mmol/L 2-DG or DMSO post LPS treatment, and then lysed with the reagents in the kit. After the reaction was completed, the absorbance values were detected and recorded using a multimode plate reader (PerkinElmer, USA). Data were processed by GraphPad Prism (version 9.5) software.

2.14. Seahorse experiment

The Seahorse XFe extracellular flux analyzer (Seahorse Bioscience, USA) was applied to detect cellular extracellular acidification rate (ECAR) and oxygen consumption rate (OCR) of RAW264.7 cells. OCR was detected using the Mito-stress test kit (103673-100, Agilent Technologies, USA), and ECAR was detected using the glycolysis stress test kit (103020-100, Agilent Technologies, USA). RAW264.7 cells were cultured in Seahorse XFe96 microplates and sequentially treated with LPS and GNA or solvent. The following experiments were conducted according to the manufacturer's instructions. Data were acquired and processed using Seahorse XFe Wave software (Agilent Technologies, USA).

2.15. Expression and purification of recombinant proteins

The coding sequences of mouse HK1 protein and cysteine-mutated HK1 (Cys684 to Ala684, pET28a-HK1-C684A) were synthesized by Sangon Biotech and cloned into the pET-28a(+) vector. The recombinant protein was expressed in *Escherichia coli* BL21 (DE3) and induced by isopropyl-β-D-thiogalactopyranoside at 18 °C for 24 h. Cell pellets were collected and resuspended with PBS buffer containing 20 mmol/L Tris−HCl (pH 7.3) and 200 mmol/L NaCl. Cell fragmentation was performed at low temperature to obtain cell lysates containing recombinant proteins. The proteins were enriched with Ni-NTA beads (SA004100, Smart-Lifesciences, Changzhou, China) and eluted with a gradient of imidazole solution. After centrifugation, the protein pellets were resuspended in PBS buffer, and concentrated to yield the recombinant proteins were obtained by exchanging the imidazole in the samples with PBS buffer and concentrating them.

2.16. Bio-layer interferometry (BLI) assay

The interactions between GNA and HK1 or HK1-C684A mutants were investigated by BLI. Briefly, freshly prepared recombinant proteins were pre-coupled to the Ni-NTA biosensor (18-5101, Sartorius, Germany), and the binding and dissociation curves were measured post GNA treatment. The binding and dissociation time was set to 90 s. Kinetic analyses were done using Octet Analysis Studio (13.0).

2.17. RNA interference and transfection

The short interfering (si) RNAs targeting HK1 were designed and synthesized by Shanghai Generay Biotech Co., Ltd. (Supporting Information Table S2). The siRNA and vectors were transfected into RAW264.7 cells by Lipofectamine 2000 (11668019, Thermo Fisher, USA). Cells transferred with siRNA were subjected to Western blotting, cellular cytokine analysis, and RT-qPCR analysis.

2.18. Isolation of mitochondria and cytoplasm

The separation of mitochondria and cytoplasm was performed using a cellular mitochondrial isolation kit (C3601, Beyotime, Shanghai, China), and the isolated mitochondria or cytoplasm were subjected to Western blotting.

2.19. Statistical analysis

Statistical analyses were performed by GraphPad Prism 9.5 software. Differences between groups were assessed using One-way ANOVA followed by Tukey's multiple comparisons test. Survival data of mice were assessed using the Kaplan−Meier method. Data are reported as mean ± standard deviation (SD). $P < 0.05$ was considered significant.

3. Results

3.1. GNA alleviates multi-organ damage in septic mice

To evaluate whether gambogenic acid (GNA) could protect mice from sepsis-induced inflammation and multi-organ damage, we pretreated mice with GNA for 3 days, followed by cecal ligation and puncture (CLP) surgery (Fig. 1A). Biochemical analysis revealed that compared to the sham surgery group, CLP surgery elevated the levels of inflammatory cytokines in the serum of mice, *i.e*., tumor necrosis factor-α (TNF-α), interleukin 6 (IL-6), and IL-1β, while GNA treatment significantly reduced the levels of those cytokines (Fig. 1B−E). Hematoxylin-eosin (HE) staining of tissue sections showed that, in comparison with control mice, those in the model group displayed multi-organ damage, including lung, liver, spleen, intestine, and kidney, characterized by disruption of normal tissue architecture and enhanced inflammatory cell infiltration, whereas GNA treatment ameliorated these pathological alterations (Fig. 1F). Strikingly, within the first 48 h after CLP surgery in mice, GNA significantly improved the survival of septic mice compared with untreated mice (Fig. 1G). These results demonstrate that GNA alleviates the inflammatory response, protects against multi-organ damage, and improves the survival of septic mice.

3.2. GNA inhibits the release of inflammatory cytokines in macrophages

To investigate the anti-inflammatory effects of GNA, we induced inflammation with LPS in RAW264.7 cells. We chose 1 μmol/L as the maximal concentration for GNA treatment to avoid substantial effects on cell viability (Supporting Information Fig. S1). We first examined the effect of different concentrations of GNA on the macrophage morphology under a microscope. Untreated control cells exhibited a round morphology without pseudopods, whereas LPS-treated cells increased in size and extended pseudopods, indicating the activation of macrophages. These morphological changes in cells were ameliorated by GNA treatment (Fig. 2A). Additionally, we observed elevated levels of nitric oxide (NO), TNF-α, IL-6, and IL-1β in the supernatant of cells after LPS stimulation, which were inhibited by GNA treatment in a dose-dependent manner (Fig. 2B−E). Subsequently, we confirmed the elevated levels of these inflammatory cytokines using RT-qPCR and found that mRNA levels of *Tnfa* and *Il6* were elevated in LPS-stimulated cells, which were restored after GNA treatment (Fig. 2F and G). These findings indicate that GNA can inhibit the expression and release of inflammatory cytokines in macrophages.

3.3. HK1 serves as a potential target of GNA

The activity-based protein profiling (ABPP) technology has unprecedented potential in identifying drug targets[33-40]. To identify the potential targets of GNA, we performed an ABPP experiment in LPS-stimulated RAW264.7 cells post GNA treatment (Fig. 3A). Considering that GNA contains a Michael acceptor group, we supposed that GNA may bind covalently with the sulfhydryl group of protein cysteine residues[41]. Therefore, we incubated LPS-stimulated RAW264.7 cells with a cysteine probe, iodoacetamide-alkyne (IAA-yne), followed by click-conjugated to the fluorescent dye TAMRA-azide and assessed the competitive binding ability of GNA with IAA-yne. Experiments performed in live cells and cell lysates consistently showed that GNA competed effectively with IAA-yne in a dose-dependent manner, suggesting the binding of GNA to protein cysteine residues (Fig. 3B and Supporting Information Fig. S2). To further confirm the binding of GNA with protein cysteine residues and clarify the exact binding sites of GNA, we employed a desthiobiotin-iodoacetamide (DBIA) probe and performed mass spectrometry-based proteomics. Cell lysates treated with or without GNA were labeled with DBIA probe, labeled peptides were enriched by beads, and subjected to mass spectrometry-based proteomics analysis (Fig. 3A). As a result, 30 differential proteins ($P_{adj} < 0.01$ and $|\text{fold change}| > 2$) were identified as the potential targets of GNA (Fig. 3C and Supporting Information Table S3). Among which, we selected a highly ranked protein, HK1, which is closely associated with glycolysis and the Warburg effect, for further target validation (Fig. 3D). The cellular thermal shift assay coupled with Western blotting (CETSA-WB) experiment showed that the expression levels of HK1 decreased along with increasing temperature, demonstrating that the thermal stability of HK1 protein deteriorates with increasing temperature. GNA treatment significantly increased its thermal stability, evidenced by higher expression levels of HK1 in the GNA treatment group than those in the DMSO treatment group, suggesting the binding between GNA and HK1 (Fig. 3E and F). In addition, the pull-down experiments confirmed that DBIA bound to HK1, and this binding was outcompeted by GNA (Fig. 3G). In line with this, the immunofluorescence assay also showed the co-localization of IAA-yne with HK1 *in situ*, and the binding of IAA-yne with HK1 was almost completely outcompeted by GNA, evidenced by weakened fluorescence intensity post GNA treatment (Fig. 3H). Taken together, these data demonstrate that GNA can bind to HK1 in LPS-stimulated macrophages.

3.4. GNA inhibits the expression and activity of HK1 and alleviates the Warburg effect

To further clarify the impact of GNA on HK1, we examined the expression levels of HK1 at both protein and mRNA levels, and the activity of HK1 post GNA treatment in RAW264.7 cells. Following LPS stimulation, the expression levels of HK1 remained unchanged at both protein and mRNA levels when compared with the vehicle group (Fig. 4A−C). However, the HK1 catalytic activity was significantly upregulated (Fig. 4D). When the cells were treated with GNA, the protein levels, mRNA levels, and catalytic activity of HK1 were significantly downregulated with dose-dependent effects, suggesting that GNA modulates HK1 *via* modulating its expression level and catalytic activity (Fig. 4A−D). HK1 is a subtype of hexokinase, catalyzing the reaction of glucose with ATP to produce glucose-6-phosphate—the first step in the glycolytic pathway[42,43]. Given the close association between HK1 and the Warburg effect, we hypothesized whether the anti-inflammatory effect of GNA was mediated through the Warburg effect. To verify our hypothesis, we examined the levels of lactic acid in RAW264.7 cells post GNA treatment. As expected, the levels of

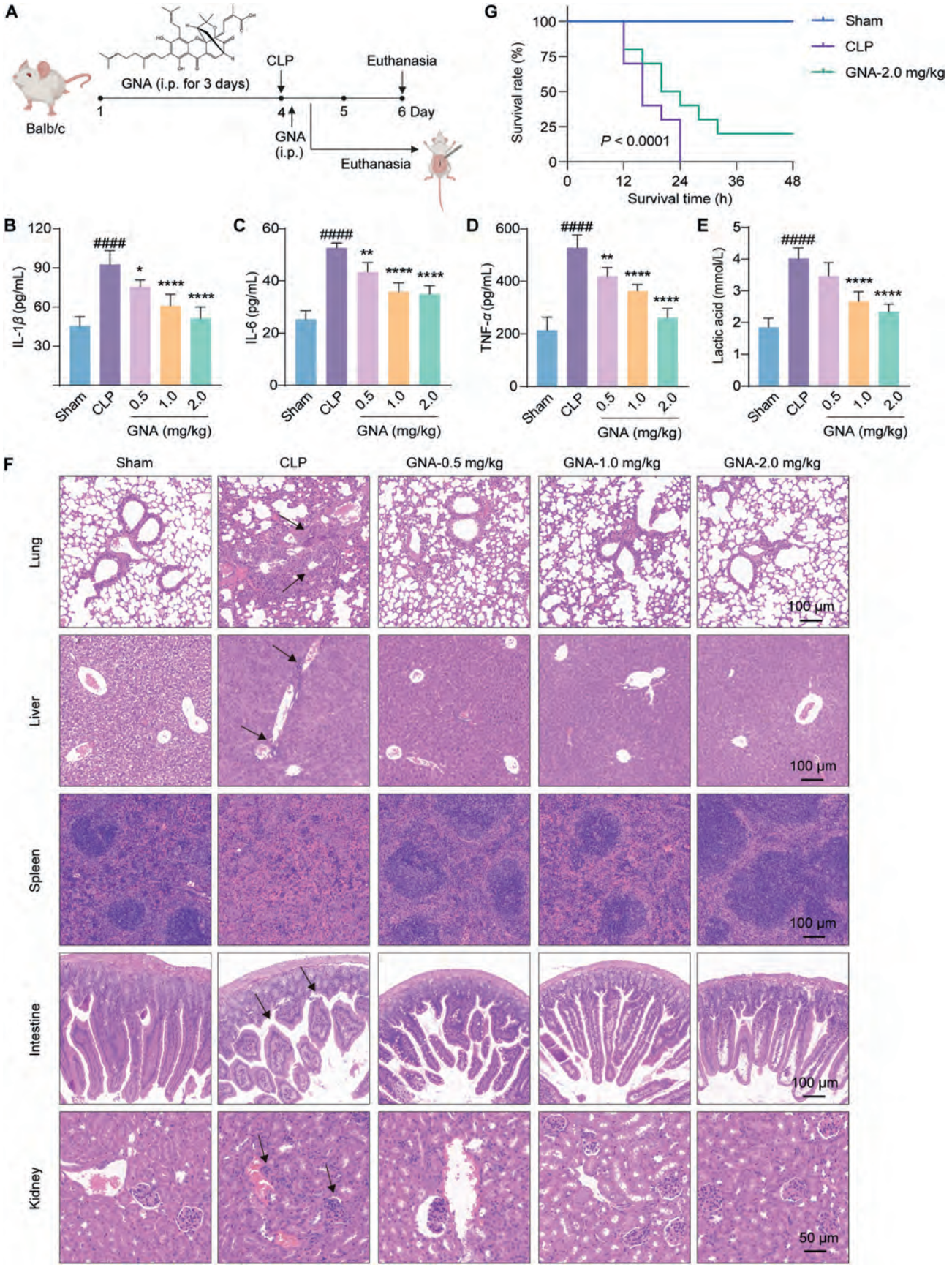

Figure 1 Gambogenic acid (GNA) attenuates multiple organ damage induced by cecum ligation and puncture in mice. (A) The scheme of the CLP-sepsis mice experiment. (B−E) Levels of interleukin-1β (IL-1β) (B), interleukin-6 (IL-6) (C), tumor necrosis factor-α (TNF-α) (D), and

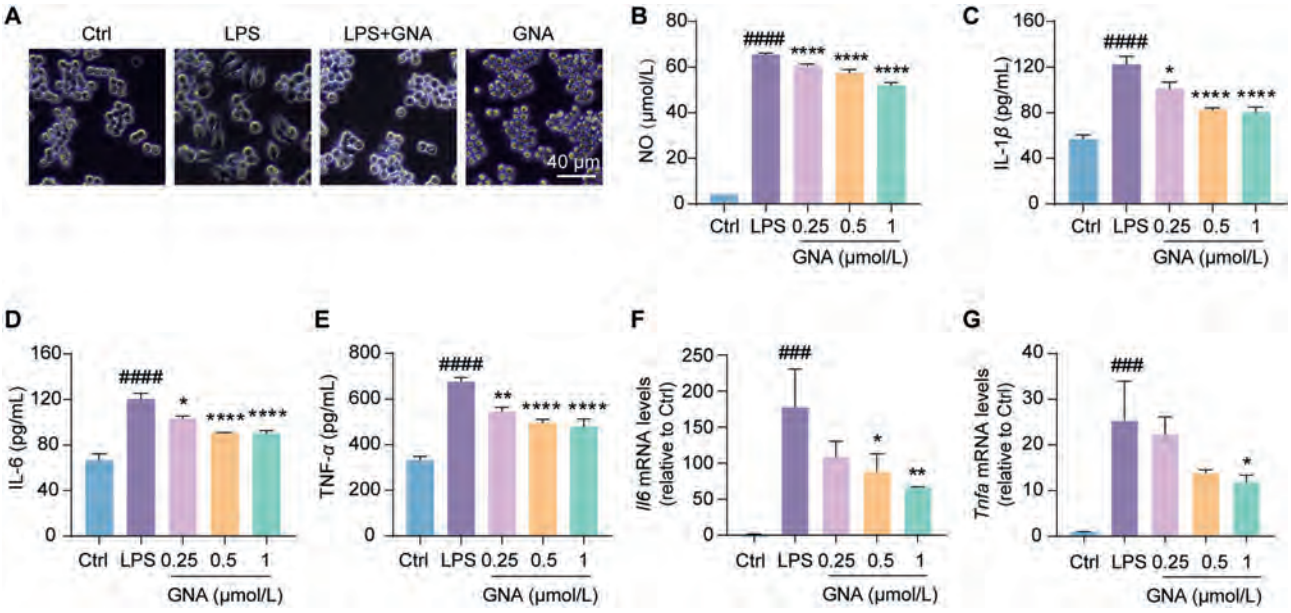

Figure 2 GNA inhibits lipopolysaccharide (LPS)-induced inflammatory responses in macrophages. (A) Photographs of RAW264.7 cells in the presence or absence of GNA for 1 h before LPS treatment for 24 h. (B−E) Levels of the inflammatory cytokines nitric oxide (NO) (B), IL-1β (C), IL-6 (D), and TNF-α (E) in the supernatants of LPS-stimulated RAW264.7 cells pretreated or untreated with GNA. $n = 3$ per group. (F, G) mRNA levels of inflammatory cytokines, *Il6* (F) and *Tnfa* (G) in LPS-stimulated RAW264.7 cells pretreated or untreated with GNA. $n = 3$ per group. Data are expressed as the mean ± SD. One-way ANOVA followed by Tukey's multiple comparisons test (B−G) was used for statistical analysis. Compared with the vehicle-treated group (Ctrl), $^{\#\#\#}P < 0.001$, $^{\#\#\#\#}P < 0.0001$. Compared with the LPS-treated group (LPS), $^{*}P < 0.05$, $^{**}P < 0.01$, $^{****}P < 0.0001$.

lactic acid were upregulated in LPS-stimulated RAW264.7 cells when compared with the vehicle group, suggesting enhanced aerobic glycolysis under inflammatory conditions, while GNA treatment alleviated the upregulated levels of lactic acid (Fig. 4E). Further examination of the energy metabolism in RAW264.7 cells revealed that GNA inhibited excessive glycolytic capacity and restored defective mitochondrial respiration induced by LPS, evidenced by changed levels of ECAR and OCR in LPS-stimulated RAW264.7 cells with/without GNA treatment (Fig. 4F−J). These findings suggest that GNA may reduce HK1 expression and activity to inhibit aerobic glycolysis in LPS-stimulated RAW264.7 cells, restoring mitochondrial respiration and thereby alleviating the Warburg effect.

3.5. *Cys684 of HK1 is the binding site for GNA*

We explored the binding of GNA with HK1 in a recombinant HK1 protein system. The recombinant HK1 protein was incubated with IAA-yne and then coupled with a fluorescent dye *via* the click reaction. With increasing concentrations of IAA-yne, the labeling reaction was carried out in a dose-dependent manner, indicating that IAA-yne could bind directly to HK1 protein (Fig. 5A). We then tested the competitiveness of GNA and IAA-yne against the recombinant HK1 protein. HK1 protein was pretreated with excessive GNA or IAA, and then incubated with IAA-yne and subjected to the click reactions. The results demonstrated that GNA effectively competed with IAA-yne for labeling of the HK1 protein, exhibiting a competitiveness comparable to that of IAA, suggesting that the reactive cysteine residue of HK1 serves as the binding site of GNA (Fig. 5B).

To identify the exact binding site, we revisited our proteomics dataset and identified the 684th cysteine residue of HK1 as the potential binding site of GNA (Fig. 5C and Supporting Information Table S1). Furthermore, molecular docking analyses revealed that the GNA can bind to the Cys684 residue of HK1 (Fig. 5D), which supports our previous finding. We then mutated Cys684 of HK1 to an Ala684 residue (C684A) and cloned a cysteine mutant variant. In IAA-yne labeling assays, the single-site mutant (C684A) HK1 proteins exhibited resistance to both GNA binding and IAA competition, indicating that the cysteine residue at position 684 is likely the critical binding site for GNA on HK1 (Fig. 5E). Next, we examined the affinity of wild-type (WT) HK1 proteins and HK1-C684A mutants for GNA by bio-layer interferometry (BLI). Results showed that the HK1-WT proteins bound and dissociated rapidly from GNA with a K_D value of 0.139 μmol/L, suggesting a strong affinity between GNA and HK1-C684A mutants (Fig. 5F). However, the HK1-C684A mutants bound and dissociated poorly from GNA with a K_D value of 196 mmol/L, suggesting a weak interaction between GNA and HK1-C684A mutants (Fig. 5G). Functionally, the catalytic activity of the HK1-

lactic acid (E) in the serum of mice post GNA treatment, $n = 5$ per group. (F) Hematoxylin-eosin (HE) staining of lung, liver, spleen, intestine, and kidney post GNA treatment, $n = 3$ per group, scale bars are indicated in figure. (G) Survival of cecal ligation and puncture (CLP) mice treated or untreated with GNA. $n = 10$ per group. Data are shown as the mean ± SD. One-way ANOVA followed by Tukey's multiple comparisons test (B−E) and the Kaplan−Meier test (G) were used for statistical analysis. Compared with the Sham group, $^{\#\#\#\#}P < 0.0001$. Compared with the CLP group, $^{*}P < 0.05$, $^{**}P < 0.01$, $^{****}P < 0.0001$.

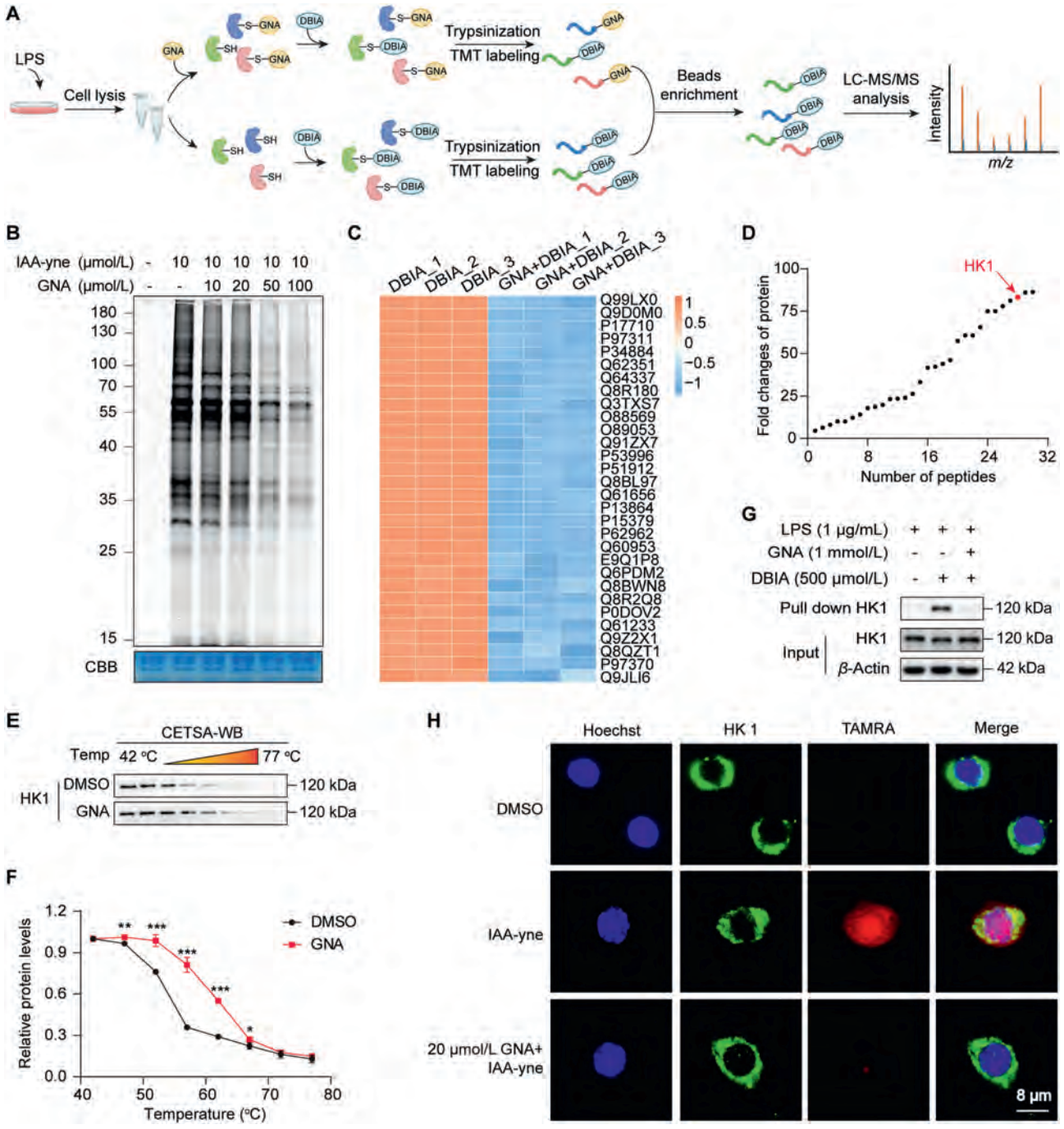

Figure 3 Identification of potential protein targets of GNA by the activity-based protein profiling (ABPP). (A) The workflow of ABPP for the profiling of GNA target proteins. (B) Competition between GNA and the iodoacetamide-alkyne (IAA-yne) probe for binding to the cysteine residues of proteins in LPS-stimulated RAW264.7 cells. (C) Heatmap of the differential proteins ($P_{adj} < 0.01$ and |fold change| > 2) between DBIA and GNA + DBIA groups. The concentration of GNA was 500 μmol/L $n = 3$ per group. (D) Rank of the differential proteins in panel (C) against peptide numbers. (E, F) Expression levels of hexokinase-1 (HK1) protein under ascending heating conditions in the presence or absence of GNA (80 μmol/L). Data are shown as the mean ± SD. One-way ANOVA followed by the multiple comparisons test method of Benjamini, Krieger, and Yekutieli was used for statistical analysis. Compared with the corresponding protein expression levels in DMSO at different temperatures, $^{*}P < 0.05$, $^{**}P < 0.01$, $^{***}P < 0.001$. (G) Pull-down assay of HK1 in the presence and absence of GNA and DBIA in LPS-stimulated RAW264.7 cells. (H) Immunofluorescence staining of HK1 (green) and IAA-yne (red), scale bar, 8 μm.

C684A mutants was significantly lower than that of HK1-WT proteins (Fig. 5H). In addition, comparable inhibitory potency was observed when GNA was co-incubated with HK1-WT proteins (Fig. 5H), indicating that the Cys684 residue site is crucial for the catalytic activity of the HK1 protein and serves as the key site through which GNA exerts its inhibitory effect on HK1 . Collectively, these results indicate that GNA binds to the Cys684 residue site of HK1 and reduces the activity of HK1.

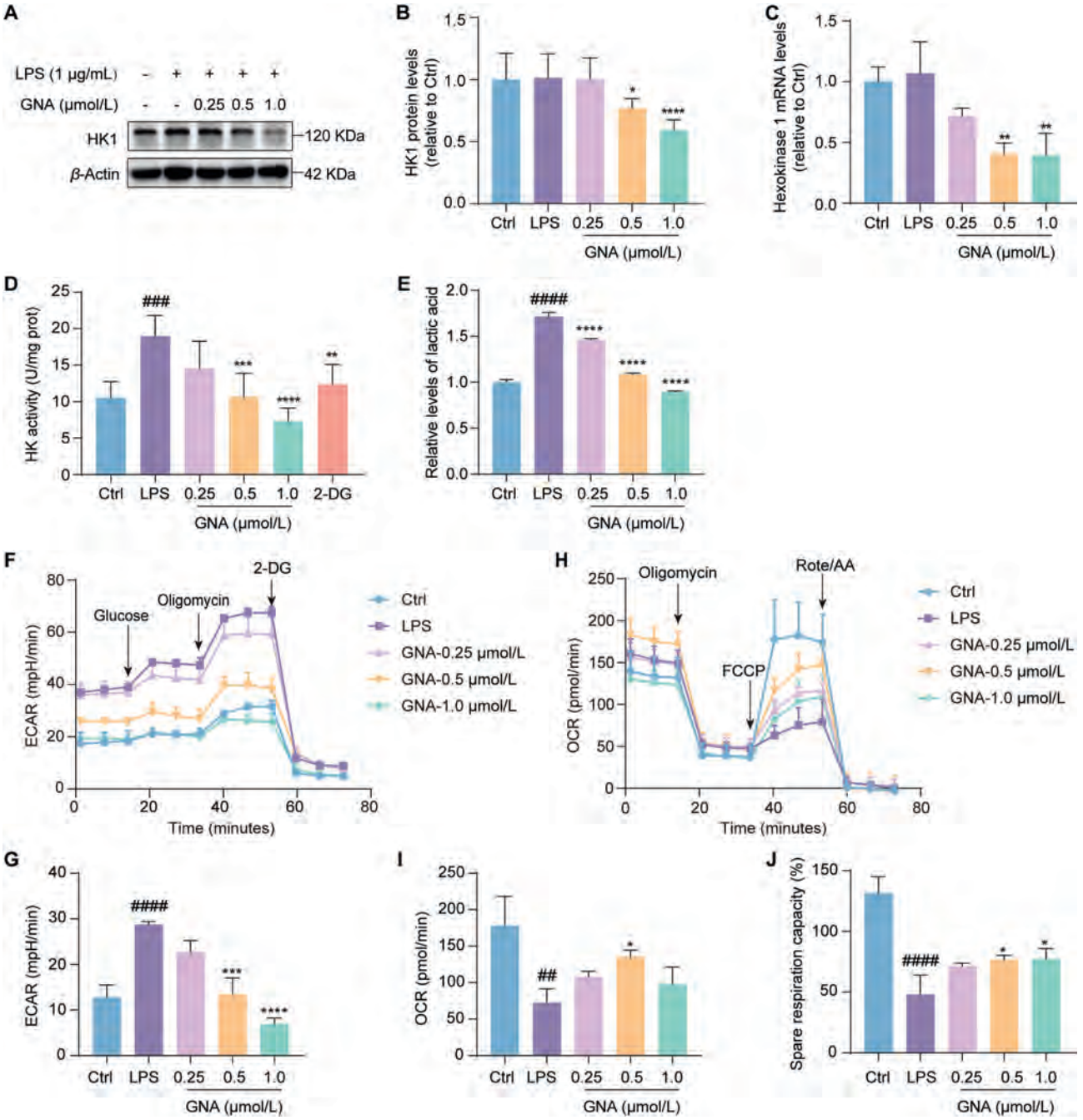

Figure 4 GNA inhibits HK1 and reduces LPS-induced Warburg effect in RAW264.7 cells. (A) Western blots of HK1 in LPS-stimulated RAW264.7 cells pretreated or untreated with GNA. (B) Densitometry analysis of the HK1 protein levels in the Western blot corresponding to panel (A), $n = 3$ per group. (C) The mRNA levels of hexokinase 1 in LPS-stimulated RAW264.7 cells pretreated or untreated with GNA, $n = 3$ per group. (D) Enzyme activity of HK in LPS-activated RAW264.7 cells pretreated or untreated with GNA, $n = 3$ per group. (E) The levels of lactic acid in LPS-activated RAW264.7 cells pretreated or untreated with GNA, $n = 3$ per group. (F, G) Extracellular acidification rate (ECAR) (F) and glycolysis capacity (G) of LPS-stimulated RAW264.7 cells treated with or without GNA, $n = 3$ per group. (H–J) The oxygen consumption rate (OCR) (H), maximal respiration (I), and spare respiration capacity (J) of LPS-activated RAW264.7 cells treated with or without GNA, $n = 3$ per group. Data are expressed as the mean ± SD. One-way ANOVA followed by Tukey's multiple comparisons test was used for statistical analysis. Compared with the Ctrl group, $^{\#\#}P < 0.01$, $^{\#\#\#}P < 0.001$, $^{\#\#\#\#}P < 0.0001$. Compared with the LPS group, $^{*}P < 0.05$, $^{**}P < 0.01$, $^{***}P < 0.001$, $^{****}P < 0.0001$.

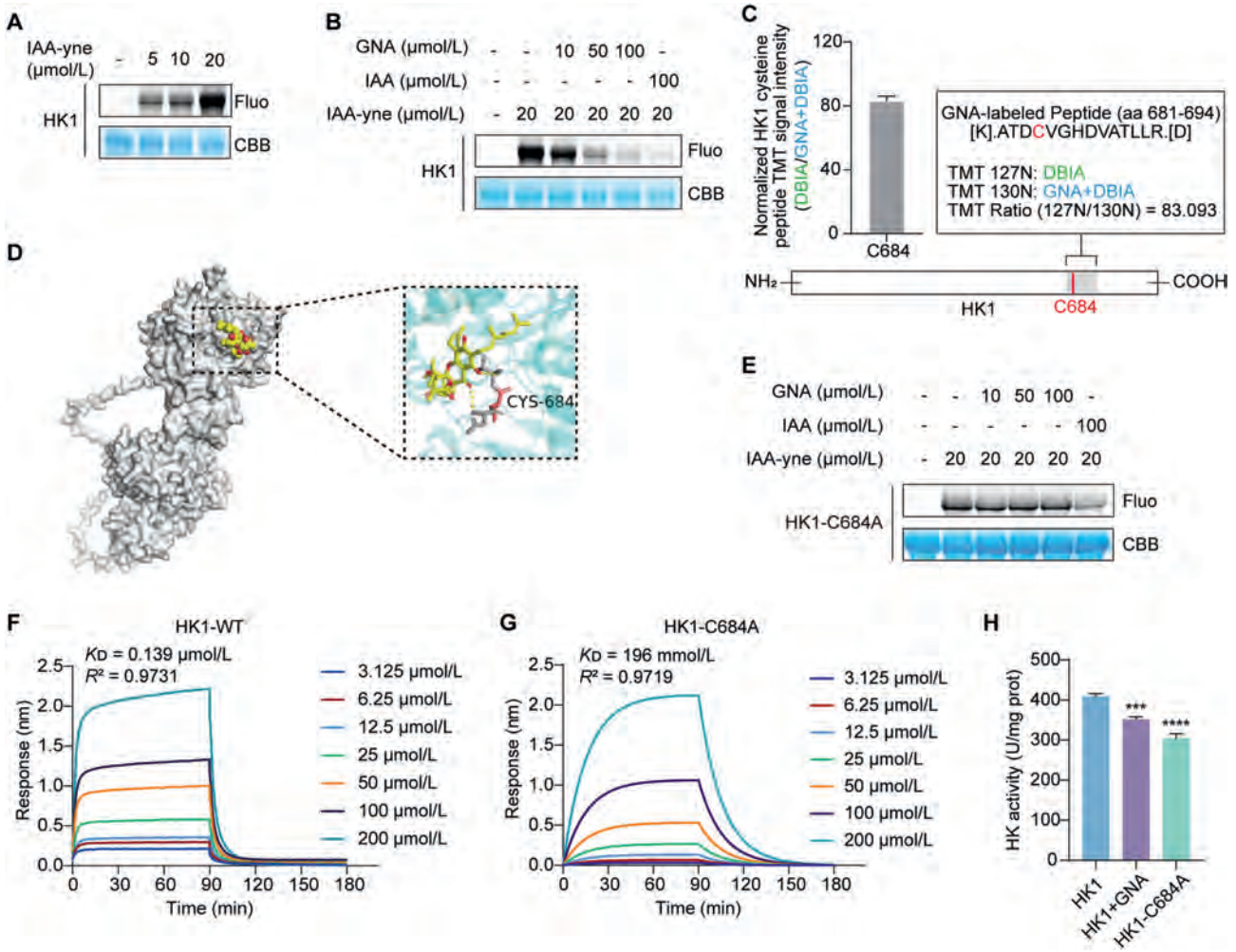

Figure 5 GNA directly binds to Cys684 residues of HK1. (A) Fluorescence labeling of recombinant mouse HK1 proteins incubated with different concentrations of IAA-yne. (B) Fluorescence labeling of IAA-yne labeled HK1 proteins in the presence or absence of the competitors GNA or IAA. (C) The binding site of GNA on HK1 protein resulted from the ABPP profiling dataset, $n = 3$ per group. (D) Molecular docking of GNA with HK1 protein. (E) Fluorescence labeling of HK1 single-site mutant (C684A) proteins incubated with IAA-yne in the presence or absence of the competitors, GNA or IAA. (F, G) Affinity of GNA to wild-type HK1 (F) and HK1-C684A mutant (G) proteins. (H) Enzyme activity of recombinant HK1-WT protein and HK1-C684A mutant proteins in the presence or absence of GNA (1 μmol/L), $n = 3$ per group. Data are expressed as the mean ± SD. One-way ANOVA followed by Tukey's multiple comparisons test was used for statistical analysis. Compared with the enzyme activity of wild-type HK1, $^{***}P < 0.001$, $^{****}P < 0.0001$.

3.6. GNA regulates HK1-mediated NLRP3 inflammasome activation

Under physiological conditions, HK is predominantly localized on the outer mitochondrial membrane[44-46]. When cells are inclined to produce energy mainly relies on glycolysis, the intracellular level of G6P increases, triggering the release of HK from mitochondria to suppress the production of G6P[47,48]. Importantly, HK dissociation from mitochondria is the upstream event in the activation of NLRP3 inflammatory vesicles[19]. To determine whether GNA alleviates the inflammatory response of LPS-stimulated macrophages by regulating the dissociation of HK1 from mitochondria, we assessed the effect of GNA treatment on the levels of HK1 in mitochondrial and cytoplasmic fractions. We found that LPS stimulation increased the cytoplasmic HK1 levels and decreased mitochondrial HK1 levels at both 6 and 12 h post-stimulation (Fig. 6A and B). Remarkably, GNA treatment gradually reduced the level of cytoplasmic HK1 with increasing treatment time, indicating that GNA inhibits the dissociation of HK1 from the mitochondrial membrane (Fig. 6A and B). Next, we investigated the downstream events of inhibiting the dissociation of HK1 by GNA, and found that the elevated protein and mRNA levels of *Nlrp3*, *Asc*, *Casp1*, and *Il1b* were reduced by GNA treatment in LPS-stimulated RAW264.7 cells (Fig. 6C−G and Supporting Information Fig. S3). Consistently, immunofluorescence results showed that LPS treatment increased NLRP3 protein expression in RAW264.7 cells, while GNA treatment decreased NLRP3 protein levels (Fig. 6H). These results suggest that LPS-induced dissociation of HK1 from mitochondria contributes to the activation of the NLRP3/Caspase-1/ASC/IL-1β cascade *in vitro*. Apart from the mechanism that GNA alleviated the Warburg effect *via* modulating the activity of HK1, here we demonstrated that GNA inhibited the dissociation of HK1 from the mitochondrial membrane, reduced the cytoplasmic levels of HK1, and therefore

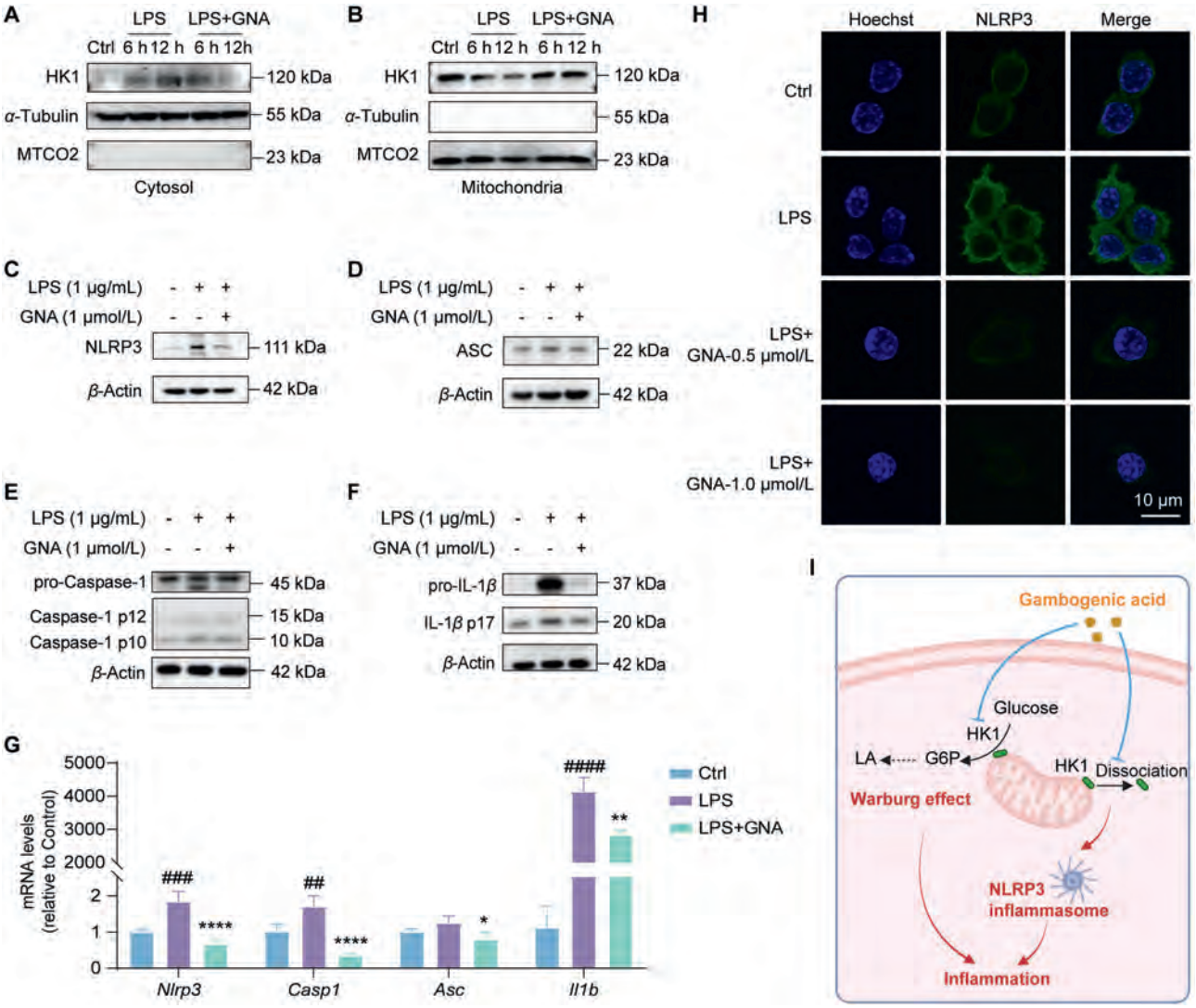

Figure 6 GNA inhibits the activation of NLR family pyrin domain containing 3 (NLRP3) inflammasome *via* regulating the dissociation of HK1 from the mitochondria. (A, B) Western blots of HK1 in the cytoplasmic (A) and mitochondrial (B) fractions of LPS-stimulated RAW264.7 cells in the presence or absence of GNA. β-Tubulin and MTCO20 were used to assess the complete separation of mitochondria from cytoplasm. (C−F) Western blots of NLRP3 (C), apoptosis-associated speck-like protein containing a CARD (ASC) (D), Caspase-1 (E), and IL-1β (F) proteins of LPS-stimulated RAW264.7 cells in the presence or absence of GNA. (G) Relative mRNA levels of *Nlrp3*, *Casp1*, *Asc*, and *Il1b* of LPS-stimulated RAW264.7 cells in the presence or absence of GNA (1 μmol/L). $n = 3$ per group. Data are expressed as the mean ± SD. One-way ANOVA followed by Tukey's multiple comparisons test was used for statistical analysis. Compared with the Ctrl group, $^{\#\#}P < 0.01$, $^{\#\#\#}P < 0.001$, $^{\#\#\#\#}P < 0.0001$. Compared with the LPS group, $^{*}P < 0.05$, $^{**}P < 0.01$, $^{****}P < 0.0001$. (H) Immunofluorescence staining of NLRP3 (green) in LPS-stimulated RAW264.7 cells in the presence or absence of GNA. Scale bar, 10 μm. (I) Mechanistic diagram of GNA inhibiting the release of inflammatory cytokines by interfering with HK1 function and localization. LA, lactic acid, G6P, glucose-6-phosphate, HK1, hexokinase 1.

suppressed the activation of NLRP3 inflammasome and the release of inflammatory cytokines (Fig. 6I).

3.7. Knockdown of HK1 attenuates the inflammatory responses in LPS-stimulated macrophages

To verify the role of HK1 in the Warburg effect and NLRP3 inflammasome activation, we transfected RAW264.7 cells with HK1 siRNAs (siHK1#1, siHK1#2, and siHK1#3), which led to a marked reduction in HK1 expression (Fig. 7A−C). As expected, knockdown of HK1 reduced the levels of ECAR and decreased intracellular lactate levels compared with the siNC group, confirming the role of HK1 in the aerobic glycolysis in LPS-stimulated macrophages (Fig. 7D−F). In addition, HK1 knockdown decreased the elevated levels of NLRP3, ASC, Caspase-1, and IL-1β in LPS-stimulated macrophages, demonstrating that the activation of NLRP3 inflammasome is mediated by HK1 (Fig. 7G−J and Supporting Information Fig. S4). Functionally, knockdown of HK1 in RAW264.7 cells reduced the LPS-induced upregulation of NO, TNF-α, IL-6, and IL-1β, suggesting the proinflammatory role of HK1 in LPS-stimulated macrophages. Moreover, treatment of HK1-knockdown cells with GNA resulted in a comparable reduction in the levels of these mediators, with the exception of NO (Fig. 7K−N). These findings confirm that the

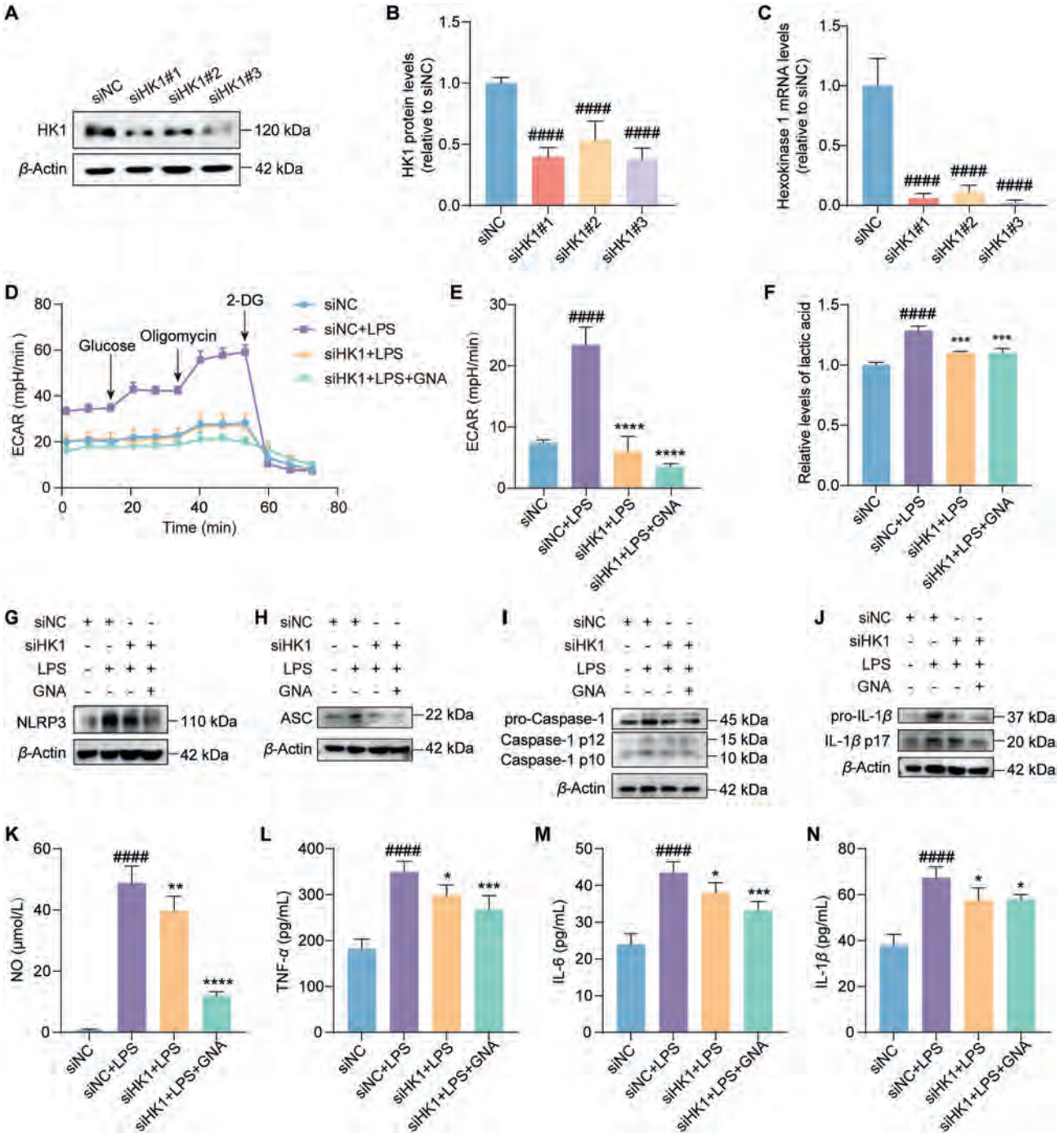

Figure 7 Gene silencing of hexokinase 1 attenuates LPS-induced Warburg effect in RAW264.7 cells and inhibits the activation of NLRP3 inflammatory vesicles. (A, B) Western blots (A) and relative protein levels (B) of HK1 in RAW264.7 cells transfected with siHK1#1, siHK1#2, or siHK1#3. $n = 3$ per group. (C) Relative mRNA levels of hexokinase 1 in RAW264.7 cells transfected with siHK1#1, siHK1#2, or siHK1#3. (D, E). ECAR (D) and glycolysis capacity (E) of RAW264.7 cells transfected with siHK1 and treated with or without GNA (1 μmol/L). $n = 3$ per group. (F) Levels of intracellular lactic acid content of RAW264.7 cells transfected with siHK1 and treated with or without GNA (1 μmol/L). $n = 3$ per group. (G–J) Western blots of NLRP3 (G), ASC (H), Caspase-1 (I), and IL-1β (J) proteins in RAW264.7 cells transfected with siHK1 and treated with or without GNA (1 μmol/L). (K–N). Levels of cytokines NO (K), TNF-α (L), IL-6 (M), and IL-1β (N) in the supernatants of LPS-stimulated RAW264.7 cells transfected with siHK1 and treated with or without GNA (1 μmol/L). $n = 5$ per group. In B, C, E, F, K–N, data are expressed as the mean ± SD. One-way ANOVA followed by Tukey's multiple comparisons test was used for statistical analysis. Compared with the siNC group, $^{\#\#\#\#}P < 0.0001$. Compared with the siNC + LPS group, $^{*}P < 0.05$, $^{**}P < 0.01$, $^{***}P < 0.001$, $^{****}P < 0.0001$.

anti-inflammatory activity of GNA is mediated through HK1. Collectively, GNA exerts anti-inflammatory effects *via* HK1-mediated Warburg effect and NLRP3 inflammasome activation.

4. Discussion

Sepsis remains a deadly threat to the geriatric and pediatric populations, as well as burn victims[49-54]. Over the past decades, attention has been paid to the in-depth studies of sepsis mechanisms and the updating of therapeutic strategies, yet there are still no targeted drugs with satisfactory efficacy[55-58]. This work revealed that GNA, a small molecule compound derived from the resin of *Garcinia hanburyi* Hook.f., significantly reduced the levels of inflammatory cytokines in the serum of CLP mice, protected them from multi-organ damage caused by inflammatory storms, and prolonged the survival of the mice. Through the combined use of chemoproteomics, CETSA, and BLI, we systematically investigated the targets and mechanisms underlying the protective effects of GNA on sepsis and found that GNA exerts anti-inflammatory effects *via* HK1-mediated Warburg effect and NLRP3 inflammasome activation.

It is well known that the Warburg effect was initially identified as a metabolic reprogramming event in tumors. Subsequent studies have revealed that the Warburg effect also plays a vital role in inflammation[59-61]. Like tumor cells, immune cells tend to rewire their metabolic processes to meet the demands of their rapid proliferation and normal function under inflammatory conditions. Metabolic reprogramming during the pathogenesis and progression of inflammation and sepsis provides novel opportunities for developing novel therapeutic strategies. Several studies have confirmed the role of the Warburg effect in sepsis[14,62-65]. Correspondingly, therapeutic strategies targeting the Warburg effect have been developed for the treatment of sepsis, including those targeting epidermal growth factor receptor (EGFR)[15], interferon-γ (IFN-γ)[66], and small molecules targeting key metabolic enzymes in aerobic glycolysis, such as Angiotensin-(1−7) (targeting HK2, PFKFB3, and PKM2)[67], Shikonin (targeting PKM2)[64], celastrol (targeting PKM2)[35], and Capsaicin (targeting PKM2 and LDHA)[34]. Here, we propose another promising small molecule, GNA, which targets HK1 in aerobic glycolysis for the treatment of inflammation and sepsis.

HK is one of the rate-limiting enzymes catalyzing the conversion of glucose to glucose-6-phosphate, the first reaction in glycolysis. It has four isozymes, among which HK1 is widely expressed in most adult tissues[68,69]. It has been reported that HK1 is a key regulator of glucose metabolism and is involved in various pathological processes (*e.g.*, inflammation, diabetes, and cancer)[69-71]. In the present study, we found that GNA inhibited the Warburg effect in LPS-stimulated RAW264.7 cells by binding to the Cys684 residue of HK1 protein and thereby suppressing HK1 function. In addition, HK1 is normally located in the outer mitochondrial membrane, but it delocalizes from the mitochondria and activates inflammasome vesicles under inflammatory conditions[19,72]. Our study found that GNA reduced LPS-induced dissociation of HK1 from mitochondria in RAW264.7 cells, thereby preventing the assembly of NLRP3 inflammasome vesicles and the secretion of IL-1β. Functionally, when we inhibited HK1 expression in RAW264.7 cells with siRNA, we observed reductions in the abnormally high levels of ECAR and inflammatory cytokines induced by LPS. Therefore, HK1 may serve as a promising target for the treatment of sepsis in the future.

Interestingly, when siHK1 cells were treated with GNA, the levels of inflammatory cytokines such as TNF-α, IL-6, and IL-1β were reduced to a degree comparable to those in untreated cells. However, GNA treatment led to a further decrease in NO levels, indicating that HK1 is a crucial yet not the sole anti-sepsis target of GNA. Consistently, our previous proteomics data identified 30 potential targets of GNA, implying that other targets besides HK1 may also contribute to the anti-sepsis mechanisms of GNA. Nevertheless, the present study demonstrates the crucial role of HK1 in LPS-induced Warburg effect and NLRP3 inflammasome activation. More importantly, we show that GNA exerts its anti-sepsis effect by inhibiting HK1-mediated Warburg effect and NLRP3 inflammasome activation.

5. Conclusions

Overall, this study expands our understanding of the beneficial effects of GNA on sepsis, as well as its potential targets and mechanisms of action. *In vitro* and *in vivo* experiments demonstrate that GNA inhibits the release of inflammatory cytokines in LPS-stimulated macrophages and protects mice against CLP-induced sepsis. Mechanistically, GNA binds to the Cys684 residue of HK1, thereby alleviating the Warburg effect. Additionally, GNA suppresses the dissociation of HK1 from mitochondria and inhibits NLRP3 inflammasome activation. Collectively, GNA attenuates inflammation by targeting HK1-mediated regulation of the Warburg effect and NLRP3 inflammasome activation, highlighting its potential as a novel therapeutic agent for sepsis and inflammatory disorders.

Acknowledgments

The work was supported by grants from the Scientific and Technological Innovation Projects of China Academy of Chinese Medical Sciences (CI2023D008, CI2023D003, CI2023E005TS03, and CI2023E005TS05, China), the Establishment of Sino-Austria "Belt and Road" Joint Laboratory on Traditional Chinese Medicine for Severe Infectious Diseases and Joint Research (2020YFE0205100, China), the National Key Research and Development Program of China (2022YFC2303603, 2020YFA0908000, and 2023YFC3503904, China), the National Natural Science Foundation of China (82304812 and 82521104, China), the Beijing Nova Program (20250484875, China), the CACMS Innovation Fund (CI2023E002, CI2024E003, and ZG2024001-05, China), and the Fundamental Research Funds for the Central public welfare research institutes (ZZ16-ND-10, ZZ16-YQ-046, ZZ17-ND-10, ZZ17-ND-10-07, ZZ18-ND-10, and ZZ18-ND-10-21, China).

Author contributions

Chengchao Xu, Jigang Wang, Xijun Wang, and Huanhuan Pang supervised the project and conceived the idea. Huanhuan Pang, Honglin Chen, Peng Chen, and Xu Wei designed and performed all the experiments and data analysis. Hongda Liu, Xueling He, Yang Yang, Linlin Lou, and Wen Xie assisted in the animal and cell experiments. Junzhe Zhang and Dianfei Li assisted in the collection and analysis of proteomic data. Chong Qiu, Fei Xia, Qiuyan Guo, and Shengnan Shen assisted in the experiment design. Huanhuan Pang and Honglin Chen wrote the paper. Qiaoli

Shi, Weiguang Li, and Guang Han edited the paper. All authors approved the final version of the manuscript.

Conflicts of interest

The authors declare no competing interests.

Appendix A. Supporting information

Supporting information to this article can be found online at https://doi.org/10.1016/j.apsb.2025.10.020.

References

1. Liu AC, Patel K, Vunikili RD, Johnson KW, Abdu F, Belman SK, et al. Sepsis in the era of data-driven medicine: personalizing risks, diagnoses, treatments and prognoses. *Briefings Bioinf* 2020;**21**: 1182−95.
2. Nedeva C. Inflammation and cell death of the innate and adaptive immune system during sepsis. *Biomolecules* 2021;**11**:1011.
3. Li DP, Wei RJ, Zhang XL, Gong SH, Wan MJ, Wang FZ, et al. Gut commensal metabolite rhamnose promotes macrophages phagocytosis by activating SLC12A4 and protects against sepsis in mice. *Acta Pharm Sin B* 2024;**14**:3068−85.
4. Fang DD, Li Y, He B, Gu DQ, Zhang MM, Guo JW, et al. Gastrin attenuates sepsis-induced myocardial dysfunction by down-regulation of TLR4 expression in macrophages. *Acta Pharm Sin B* 2023;**13**: 3756−69.
5. Rudd KE, Johnson SC, Agesa KM, Shackelford KA, Tsoi D, Kievlan DR, et al. Global, regional, and national sepsis incidence and mortality, 1990-2017: analysis for the global Burden of Disease Study. *Lancet* 2020;**395**:200−11.
6. Oussalah A, Callet J, Manteaux AE, Thilly N, Jay N, Guéant JL, et al. Usefulness of procalcitonin at admission as a risk-stratifying biomarker for 50-day in-hospital mortality among patients with community-acquired bloodstream infection: an observational cohort study. *Biomark Res* 2023;**11**:4.
7. Balch JA, Chen UI, Liesenfeld O, Starostik P, Loftus TJ, Efron PA, et al. Defining critical illness using immunological endotypes in patients with and without sepsis: a cohort study. *Crit Care* 2023;**27**:292.
8. Liu D, Huang SY, Sun JH, Zhang HC, Cai QL, Gao C, et al. Sepsis-induced immunosuppression: mechanisms, diagnosis and current treatment options. *Mil Med Res* 2022;**9**:56.
9. Cecconi M, Evans L, Levy M, Rhodes A. Sepsis and septic shock. *Lancet* 2018;**392**:75−87.
10. Evans L, Rhodes A, Alhazzani W, Antonelli M, Coopersmith CM, French C, et al. Surviving sepsis campaign: international guidelines for management of sepsis and septic shock 2021. *Intensive Care Med* 2021;**47**:1181−247.
11. Zhang YY, Ning BT. Signaling pathways and intervention therapies in sepsis. *Signal Transduct Target Ther* 2021;**6**:407.
12. Esposito S, De Simone G, Boccia G, De Caro F, Pagliano P. Sepsis and septic shock: new definitions, new diagnostic and therapeutic approaches. *J Glob Antimicrob Resist* 2017;**10**:204−12.
13. Atreya MR, Wong HR. Precision medicine in pediatric sepsis. *Curr Opin Pediatr* 2019;**31**:322−7.
14. Pan TT, Sun SQ, Chen Y, Tian R, Chen EZ, Tan RM, et al. Immune effects of PI3K/Akt/HIF-1α-regulated glycolysis in polymorphonuclear neutrophils during sepsis. *Crit Care* 2022;**26**:29.
15. Huang L, Zhang XD, Fan JY, Liu XL, Luo SH, Cao DQ, et al. EGFR promotes the apoptosis of $CD4^+$ T lymphocytes through TBK1/Glut1 induced Warburg effect in sepsis. *J Adv Res* 2023;**44**:39−51.
16. De Jesus A, Keyhani-Nejad F, Pusec CM, Goodman L, Geier JA, Stoolman JS, et al. Hexokinase 1 cellular localization regulates the metabolic fate of glucose. *Mol Cell* 2022;**82**:1261−77.e9.
17. Xu S, Herschman HR. A tumor agnostic therapeutic strategy for hexokinase 1-Null/Hexokinase 2-positive cancers. *Cancer Res* 2019; **79**:5907−14.
18. Šimčíková D, Gardáš D, Hložková K, Hruda M, Žáček P, Rob L, et al. Loss of hexokinase 1 sensitizes ovarian cancer to high-dose metformin. *Cancer Metabol* 2021;**9**:41.
19. Wolf AJ, Reyes CN, Liang W, Becker C, Shimada K, Wheeler ML, et al. Hexokinase is an innate immune receptor for the detection of bacterial peptidoglycan. *Cell* 2016;**166**:624−36.
20. Baik SH, Ramanujan VK, Becker C, Fett S, Underhill DM, Wolf AJ. Hexokinase dissociation from mitochondria promotes oligomerization of VDAC that facilitates NLRP3 inflammasome assembly and activation. *Sci Immunol* 2023;**8**:eade7652.
21. Zhang XW, Wang RH, Hu D, Sun XY, Fujioka H, Lundberg K, et al. Oligodendroglial glycolytic stress triggers inflammasome activation and neuropathology in Alzheimer's disease. *Sci Adv* 2020;**6**:eabb8680.
22. Fu JN, Wu H. Structural mechanisms of NLRP3 inflammasome assembly and activation. *Annu Rev Immunol* 2023;**41**:301−16.
23. Mangan MSJ, Olhava EJ, Roush WR, Seidel HM, Glick GD, Latz E. Targeting the NLRP3 inflammasome in inflammatory diseases. *Nat Rev Drug Discov* 2018;**17**:688.
24. Dong ST, Guo XN, Han F, He ZG, Wang YJ. Emerging role of natural products in cancer immunotherapy. *Acta Pharm Sin B* 2022;**12**: 1163−85.
25. Zhu YY, Ouyang ZJ, Du HJ, Wang MJ, Wang JJ, Sun HY, et al. New opportunities and challenges of natural products research: when target identification meets single-cell multiomics. *Acta Pharm Sin B* 2022; **12**:4011−39.
26. Huang Q, Guo KK, Ren YT, Tan JQ, Ren Y, Zhang L, et al. Design, synthesis, and biological evaluation of gambogenic acid derivatives: unraveling their anti-cancer effects by inducing pyroptosis. *Bioorg Chem* 2024;**145**:107182.
27. Xu LF, Meng XX, Xu NH, Fu WW, Tan HS, Zhang L, et al. Gambogenic acid inhibits fibroblast growth factor receptor signaling pathway in erlotinib-resistant non-small-cell lung cancer and suppresses patient-derived xenograft growth. *Cell Death Dis* 2018;**9**: 262.
28. Huang TT, Zhang HM, Wang XY, Xu L, Jia JF, Zhu XL. Gambogenic acid inhibits the proliferation of small-cell lung cancer cells by arresting the cell cycle and inducing apoptosis. *Oncol Rep* 2019;**41**: 1700−6.
29. Zhao Q, Zhong J, Bi Y, Liu YQ, Liu YX, Guo J, et al. Gambogenic acid induces Noxa-mediated apoptosis in colorectal cancer through ROS-dependent activation of IRE1α/JNK. *Phytomedicine* 2020;**78**: 153306.
30. Wu JJ, Wang DJ, Zhou JY, Li JT, Xie RX, Li YY, et al. Gambogenic acid induces apoptosis and autophagy through ROS-mediated endoplasmic reticulum stress *via* JNK pathway in prostate cancer cells. *Phytother Res* 2023;**37**:310−28.
31. Tao SB, Yang LN, Wu CZ, Hu Y, Guo F, Ren Q, et al. Gambogenic acid alleviates kidney fibrosis *via* epigenetic inhibition of EZH2 to regulate Smad7-dependent mechanism. *Phytomedicine* 2022;**106**: 154390.
32. Yu XJ, Zhao Q, Zhang HW, Fan CX, Zhang XX, Xie Q, et al. Gambogenic acid inhibits LPS-simulated inflammatory response by suppressing NF-κB and MAPK in macrophages. *Acta Biochim Biophys Sin* 2016;**48**:454−61.
33. Zhang Y, Zhang QY, Chu Z, Chen L, Chen JY, Yang Y, et al. Oridonin acts as a novel senolytic by targeting glutathione *S*-transferases to activate the ROS−p38 signaling axis in senescent cells. *Chem Commun* 2022;**58**:13250−3.
34. Zhang Q, Luo P, Xia F, Tang H, Chen JY, Zhang JZ, et al. Capsaicin ameliorates inflammation in a TRPV1-independent mechanism by inhibiting PKM2−LDHA-mediated Warburg effect in sepsis. *Cell Chem Biol* 2022;**29**:1248−59.e6.
35. Luo P, Zhang Q, Zhong TY, Chen JY, Zhang JZ, Tian Y, et al. Celastrol mitigates inflammation in sepsis by inhibiting the PKM2-dependent Warburg effect. *Mil Med Res* 2022;**9**:22.

36. Luo P, Liu D, Zhang Q, Yang F, Wong YK, Xia F, et al. Celastrol induces ferroptosis in activated HSCs to ameliorate hepatic fibrosis *via* targeting peroxiredoxins and HO-1. *Acta Pharm Sin B* 2022;**12**: 2300−14.
37. Chen JY, Gao P, Xiao W, Cheng GQ, Krishna S, Wang JY, et al. Multi-omics dissection of stage-specific artemisinin tolerance mechanisms in Kelch13-mutant Plasmodium falciparum. *Drug Resist Updates* 2023; **70**:100978.
38. Gao P, Wang JY, Qiu C, Zhang HM, Wang C, Zhang Y, et al. Photoaffinity probe-based antimalarial target identification of artemisinin in the intraerythrocytic developmental cycle of *Plasmodium falciparum*. *Imeta* 2024;**3**:e176.
39. Qiu C, Xia F, Zhang JZ, Shi QL, Meng YQ, Wang C, et al. *Advanced strategies for overcoming endosomal/lysosomal barrier in nanodrug delivery*, **6**. Research (Wash D C); 2023. p. 148.
40. Wang J, Zhang CJ, Chia WN, Loh CC, Li Z, Lee YM, et al. Haem-activated promiscuous targeting of artemisinin in *Plasmodium falciparum. Nat Commun* 2015;**6**:10111.
41. Wang X, Cao W, Zhang JJ, Yan M, Xu Q, Wu XB, et al. A covalently bound inhibitor triggers EZH2 degradation through CHIP-mediated ubiquitination. *EMBO J* 2017;**36**:1243−60.
42. Seiler K, Humbert M, Minder P, Mashimo I, Schläfli AM, Krauer D, et al. Hexokinase 3 enhances myeloid cell survival *via* non-glycolytic functions. *Cell Death Dis* 2022;**13**:448.
43. Fang J, Luo SD, Lu ZM. HK2: gatekeeping microglial activity by tuning glucose metabolism and mitochondrial functions. *Mol Cell* 2023;**83**:829−31.
44. Bantug GR, Fischer M, Grählert J, Balmer ML, Unterstab G, Develioglu L, et al. Mitochondria-endoplasmic reticulum contact sites function as immunometabolic hubs that orchestrate the rapid recall response of memory $CD8^+$ T cells. *Immunity* 2018;**48**: 542−55.e6.
45. Gautier B, Forêt Jacquard M, Guelfi S, Abbou S, Gonzalez E, Berthelot J, et al. Mapping the N-terminal hexokinase-I binding site onto voltage-dependent anion channel-1 to block peripheral nerve demyelination. *J Med Chem* 2022;**65**:11633−47.
46. Lin WJ, Shi WP, Ge WY, Chen LL, Guo WH, Shang P, et al. *Magnetic fields reduce apoptosis by suppressing phase separation of Tau-441*, **6**. Research (Wash D C); 2023. p. 146.
47. Hingst JR, Bjerre RD, Wojtaszewski JFP, Jensen J. Rapid radiochemical filter paper assay for determination of hexokinase activity and affinity for glucose-6-phosphate. *J Appl Physiol* 2019;**127**:661−7. 1985.
48. Tan VP, Miyamoto S. HK2/hexokinase-II integrates glycolysis and autophagy to confer cellular protection. *Autophagy* 2015;**11**:963−4.
49. Rowe TA, McKoy JM. Sepsis in older adults. *Infect Dis Clin* 2017;**31**: 731−42.
50. Simonsen KA, Anderson-Berry AL, Delair SF, Davies HD. Early-onset neonatal sepsis. *Clin Microbiol Rev* 2014;**27**:21−47.
51. Plunkett A, Tong J. Sepsis in children. *BMJ* 2015;**350**:h3017.
52. Wheeler DS, Wong HR. Sepsis in pediatric cardiac intensive care. *Pediatr Crit Care Med* 2016;**17**:S266−71.
53. Klein HJ, Niggemann P, Buehler PK, Lehner F, Schweizer R, Rittirsch D, et al. Pancreatic stone protein predicts sepsis in severely burned patients irrespective of trauma severity: a monocentric observational study. *Ann Surg* 2021;**274**:e1179−86.
54. Deitch EA, Bridges RM, Dobke M, McDonald JC. Burn wound sepsis may be promoted by a failure of local antibacterial host defenses. *Ann Surg* 1987;**206**:340−8.
55. Adelman MW, Woodworth MH, Langelier C, Busch LM, Kempker JA, Kraft CS, et al. The gut microbiome's role in the development, maintenance, and outcomes of sepsis. *Crit Care* 2020;**24**:278.
56. Hotchkiss RS, Moldawer LL, Opal SM, Reinhart K, Turnbull IR, Vincent JL. Sepsis and septic shock. *Nat Rev Dis Primers* 2016;**2**:16045.
57. Zarbock A, Nadim MK, Pickkers P, Gomez H, Bell S, Joannidis M, et al. Sepsis-associated acute kidney injury: consensus report of the 28th Acute Disease Quality Initiative workgroup. *Nat Rev Nephrol* 2023;**19**:401−17.
58. Póvoa P, Coelho L, Dal-Pizzol F, Ferrer R, Huttner A, Conway Morris A, et al. How to use biomarkers of infection or sepsis at the bedside: guide to clinicians. *Intensive Care Med* 2023;**49**:142−53.
59. Li XL, Yang YY, Zhang B, Lin XT, Fu XX, An Y, et al. Lactate metabolism in human health and disease. *Signal Transduct Target Ther* 2022;**7**:305.
60. Aounallah M, Dagenais-Lussier X, El-Far M, Mehraj V, Jenabian MA, Routy JP, et al. Current topics in HIV pathogenesis, part 2: inflammation drives a Warburg-like effect on the metabolism of HIV-infected subjects. *Cytokine Growth Factor Rev* 2016;**28**: 1−10.
61. Kelly B, O'Neill LA. Metabolic reprogramming in macrophages and dendritic cells in innate immunity. *Cell Res* 2015;**25**:771−84.
62. Liu CH, Wei W, Huang YX, Fu P, Zhang L, Zhao YL. Metabolic reprogramming in septic acute kidney injury: pathogenesis and therapeutic implications. *Metabolism* 2024;**158**:155974.
63. Bar-Or D, Carrick M, Tanner 2nd A, Lieser MJ, Rael LT, Brody E. Overcoming the Warburg effect: is it the key to survival in sepsis?. *J Crit Care* 2018;**43**:197−201.
64. Yang LC, Xie M, Yang MH, Yu Y, Zhu S, Hou W, et al. PKM2 regulates the Warburg effect and promotes HMGB1 release in sepsis. *Nat Commun* 2014;**5**:4436.
65. Srivastava A, Mannam P. Warburg revisited: lessons for innate immunity and sepsis. *Front Physiol* 2015;**6**:70.
66. Fu XZ, Wang Y. Interferon-γ regulates immunosuppression in septic mice by promoting the Warburg effect through the PI3K/AKT/mTOR pathway. *Mol Med* 2023;**29**:95.
67. Yu D, Huang WH, Sheng M, Zhang S, Pan H, Ren FF, et al. Angiotensin-(1−7) modulates the Warburg effect to alleviate inflammation in LPS-induced macrophages and septic mice. *J Inflamm Res* 2024;**17**: 469−85.
68. Chen QT, Zhang ZY, Huang QL, Chen HZ, Hong WB, Lin T, et al. HK1 from hepatic stellate cell-derived extracellular vesicles promotes progression of hepatocellular carcinoma. *Nat Metab* 2022;**4**:1306−21.
69. Wakeling MN, Owens NDL, Hopkinson JR, Johnson MB, Houghton JAL, Dastamani A, et al. Non-coding variants disrupting a tissue-specific regulatory element in HK1 cause congenital hyperinsulinism. *Nat Genet* 2022;**54**:1615−20.
70. Chen YY, Yang C, Zou M, Wang D, Sheng RL, Zhan M, et al. Inhibiting mitochondrial inflammation through Drp1/HK1/NLRP3 pathway: a mechanism of alpinetin attenuated aging-associated cognitive impairment. *Phytother Res* 2023;**37**:2454−71.
71. Hou YC, Zhang QW, Pang WJ, Hou LD, Liang Y, Han X, et al. YTHDC1-mediated augmentation of miR-30d in repressing pancreatic tumorigenesis *via* attenuation of RUNX1-induced transcriptional activation of Warburg effect. *Cell Death Differ* 2021;**28**:3105−24.
72. Sundaram SM, Doughty LA, Sereda MW. Location matters: hexokinase 1 in glucose metabolism and inflammation. *Trends Endocrinol Metabol* 2022;**33**:665−7.
73. Chen J, Bai Y, He X, Xiao W, Chen L, Wong YK, et al. The spatiotemporal transcriptional profiling of murine brain during cerebral malaria progression and after artemisinin treatment. *Nat Commun* 2025;**16**:1540.
74. Gao P, Liu YQ, Xiao W, Xia F, Chen JY, Gu LW, et al. Identification of antimalarial targets of chloroquine by a combined deconvolution strategy of ABPP and MS-CETSA. *Mil Med Res* 2022;**9**:30.
75. Guo Q, Wang Q, Chen J, Zhao M, Lu T, Guo Z, et al. Dihydroartemisinin regulated the MMP-mediated cellular microenvironment to alleviate rheumatoid arthritis. *Research (Wash D C)* 2024;**7**: 0459.
76. Kuljanin M, Mitchell DC, Schweppe DK, Gikandi AS, Nusinow DP, Bulloch NJ, et al. Reimagining high-throughput profiling of reactive cysteines for cell-based screening of large electrophile libraries. *Nat Biotechnol* 2021;**39**:630−41.
77. Tang H, Zhang Y, Yang T, Wang C, Zhu YH, Qiu LJ, et al. Cholesterol modulates the physiological response to nanoparticles by changing the composition of protein corona. *Nat Nanotechnol* 2023;**18**:1067−77.